Chapter 8

GRAVITY WAVES AND INSTABILITIES IN THE LOWER AND MIDDLE ATMOSPHERE

Jürgen Klostermeyer

Max-Planck-Institut für Aeronomie, 3411 Katlenburg-Lindau, FRG

1. INTRODUCTION

The atmosphere moves ceaselessly on scales ranging from the dimension of the earth down to the mean free path of individual air molecules. An understanding of atmospheric motions requires the study of very specific problems that have to be idealized to focus attention on the basic dynamical processes, and thus are not faithful in detail. MST radar observations comprise large-scale processes like longitudinally averaged wind fields, planetary and tidal waves, and synoptic weather disturbances, mesoscale processes like narrow jet streams, frontal zones and atmospheric gravity waves, and small-scale processes like Kelvin-Helmholtz instability and turbulence preferably at scales equal to half the radar wavelength. All these processes interact nonlinearly, e.g. winds can enhance gravity waves and gravity waves can accelerate winds (wave-mean flow interaction) or a gravity wave at a given wavelength and period can enhance gravity waves at other wavelengths and periods (wave-wave interaction). Idealizing a problem then means that some linear terms in the hydrodynamic equations are neglected to suppress unwanted types of motion and that nonlinear terms are neglected or simplified to study particular types of interaction with relatively simple mathematical tools.

It is clearly impossible to discuss the whole variety of atmospheric motions in this lecture, therefore we will confine ourselves to some basic aspects of mesoscale and small-scale gravity waves and instability mechanisms. These processes can be (and partly have been) investigated by single ST or MST radars rather than expensive networks of radars and other techniques that would be necessary to study details of large-scale processes (the physics of planetary waves, for example, depends strongly on the zonal flow averaged around a latitude circle and thus cannot be investigated by measuring only the time-averaged flow over a single radar station).

Internal gravity waves with wavelengths between ten and less than one kilometer and periods between several hours and several minutes appear to play a central role in atmospheric wavenumber and frequency spectra (VANZANDT, 1982). Therefore we discuss the propagation of gravity waves in simplified atmospheric models in Section 2. Their interaction with the wind, their mutual interaction and instability mechanisms based upon these processes will be treated in Sections 3 and 4. All sections stress the theoretical aspects but are completed by MST radar observations

showing the relevant hydrodynamic processes. Such a short treatment necessarily must be incomplete and sketchy but hopefully will stimulate further studies of dynamic processes by means of MST radars and other methods.

2. ATMOSPHERIC GRAVITY WAVES

To study atmospheric gravity waves it is convenient to consider an unbounded non-rotating model atmosphere without molecular viscosity and thermal conductivity. Thereby we eliminate unwanted types of dynamic processes like gyroscopic or inertial waves, viscosity waves and heat conduction waves resulting, respectively, from the Coriolis force and the dissipative terms in the equations of momentum and energy which play no role at the wavelengths and frequencies considered below. For further details of these wavetypes see VOLLAND (1969) and LEBLOND and MYSAK (1978). The remaining waves that can propagate through the model atmosphere fall into two categories: High-frequency acoustic waves due to the compressibility of the air and low-frequency internal gravity waves due to the gravitational force. The periods and wavelengths of acoustic waves are smaller than about 1 s and 300 m, respectively, whereas the corresponding values for internal gravity waves are larger than about 300 s and 300 m. The dispersion curves of both wave types thus are widely separated in the frequency-wavenumber plane and interactions can in general be neglected. We can therefore eliminate acoustic waves by assuming that the model atmosphere is incompressible so that the sound speed is infinite and the density cannot vary along the path of an air parcel:

$$\frac{d\rho}{dt} = 0 \tag{1}$$

where $d/dt = \partial/\partial t + \mathbf{u} \cdot \nabla$ and ρ and $\mathbf{u}$ denote density and fluid velocity. It should be mentioned, however, that this approximation also filters out long-period Lamb waves which propagate horizontally at the speed of sound and sometimes play a dominant role in the atmospheric response to tropospheric excitations (KLOSTERMEYER, 1977; LIU et al., 1982).

Together with (1), the continuity equation and the Euler equation yield a closed set of equations for describing the dynamics of the model atmosphere:

$$\nabla \cdot \mathbf{u} = 0 \tag{2}$$

$$\rho \frac{d\mathbf{u}}{dt} + \nabla p - \rho \mathbf{g} = 0 \tag{3}$$

where p and $\mathbf{g}$ denote pressure and gravitational acceleration.

Often it is useful to compare the actual atmospheric state with a reference state defined by hydrostatic equilibrium

$$\rho = \rho_0(z), \quad p = p_0(z), \quad \mathbf{u} \equiv 0 \tag{4}$$

satisfying (1) and (2) while (3) reduces to

$$p_{0z} = -\rho_0 g. \tag{5}$$

Here and in the following, the subscripts x, z and t denote partial derivatives with respect to horizontal and vertical coordinates and time, respectively. Equation (5) yields $p_0(z)$ for any given density distribution $\rho_0(z)$. An important quantity of the equilibrium state is the Väisälä-Brunt frequency N given by

$$N^2 = -g\frac{\rho_{0z}}{\rho_0}. \tag{6}$$

It will be shown below that N is the angular frequency of an air parcel when it is vertically displaced from its equilibrium position to a slightly higher or lower level. The period $2\pi/N$ is about 5 to 10 min in the earth's atmosphere. $N^2 < 0$ (convection) means that the air parcel would continue to rise or fall rather than oscillate around its equilibrium position. Such unstable situation in general cannot persist because this so-called static instability is eliminated by strong vertical mixing as fast as it forms.

Small departures from the basic state (4) can be described by the perturbation density ρ_1, pressure p_1 and velocity $\mathbf{u}_1$ defined by

$$\rho = \rho_0 + \rho_1, \quad p = p_0 + p_1, \quad \mathbf{u} = \mathbf{u}_1. \tag{7}$$

Substituting into (1)-(3) and neglecting terms containing productes of perturbation quantities yields

$$\rho_{1t} + w_1\rho_{0z} = 0 \tag{8}$$

$$\nabla \cdot \mathbf{u}_1 = 0 \tag{9}$$

$$\mathbf{u}_{1t} + \frac{1}{\rho_0}\nabla p_1 - \frac{\rho_1}{\rho_0}\mathbf{g} = 0 \tag{10}$$

where w_1 is the vertical component of $\mathbf{u}_1$. Equation (10) indicates that a reduced gravitational acceleration (or buoyancy) $\mathbf{g}\rho_1/\rho_o$ and a modified pressure p_1 act upon a displaced parcel. In a stably stratified atmosphere, buoyancy pulls back any parcel to its equilibrium position giving rise to internal wave oscillations. Linearization is primarily an approximation dictated by our inability to treat nonlinear problems with adequate mathematical tools. It is valid for wave motions of infinitesimal amplitude implying that the fluid velocity must be much smaller than the phase velocity, and clearly filters out all nonlinear interactions between waves of different wavelengths

and periods as well as self-interaction.

It is convenient to eliminate the variables ρ_1, p_1 and u_1 (the horizontal component of $\mathbf{u}_1$) yielding an equation for w_1 alone:

$$\nabla^2 w_{1tt} + N^2 \nabla_h^2 w_1 - \frac{N^2}{g} w_{1ztt} = 0 \tag{11}$$

where $\nabla_h = (\partial/\partial x, \partial/\partial y, 0)$. For constant Väisälä-Brunt frequency N, (11) has plane wave solutions of the form

$$w_1 = W_1 e^{i(lx+Mz-\omega t)}. \tag{12}$$

Then the dispersion relation

$$\left(1 - \frac{N^2}{\omega^2}\right) l^2 + \left(i\frac{N^2}{g} + M\right) M = 0 \tag{13}$$

must hold for a nontrivial solution.

The imaginary term in (13) is a consequence of the fact that for constant N, the unperturbed density ρ_0 decreases exponentially with height while the wave energy density should remain uniform in the absence of energy sources. Equation (6) in fact yields

$$\rho_0(z) = \rho_0(0) e^{-\frac{z}{H}} \tag{14}$$

where $H = g/N^2$ is the density scale height. To derive the perturbation energy density we note that the vertical displacement ζ of a fluid parcel from its equilibrium level is given by

$$\zeta_t = w_1 \tag{15}$$

so that integrating (8) with respect to time yields

$$\rho_1 = \frac{\rho_0}{H}\zeta. \tag{16}$$

From the scalar product of $\mathbf{u}_1$ with (10), and from (15) and (16) we then obtain

$$\left[\frac{\rho_0}{2}(\mathbf{u}_1^2 + N^2\zeta^2)\right]_t + \nabla \cdot (p_1 \mathbf{u}_1) = 0 \tag{17}$$

where $\rho_0 \mathbf{u}_1^2/2$ and $\rho_0 N^2 \zeta^2/2$ are the kinetic and potential wave energy densities and $p\mathbf{u}_1$ is the energy flux up to an arbitrary nondivergent contribution. The average kinetic and potential energy densities are equal, and the average wave energy density E varies as (ECKART, 1960)

$$E \propto \rho_0(z)|w_1|^2. \tag{18}$$

Constant E thus requires

$$w_1 \propto e^{\frac{z}{2H}}. \tag{19}$$

Indeed, with $M = \mathrm{Re}M + i\mathrm{Im}M$ we obtain from (13)

$$\mathrm{Im}M = -\frac{1}{2H} \tag{20}$$

and with $m = \mathrm{Re}M$

$$\omega^2 = \frac{l^2}{l^2 + m^2 + \frac{1}{4H^2}} N^2. \tag{21}$$

The frequency is zero for vertical phase propagation ($l = 0$) and equal to N for horizontal phase propagation ($m = 0$) if $l^2 >> 1/4H^2$. For $\omega > N$, no waves are possible. The hyperbolae (dashed curves) in Figure 1a represent contours of constant ω in the wavenumber domain. The group velocity

$$\mathbf{c}_g = (\frac{\partial \omega}{\partial l}, \frac{\partial \omega}{\partial m}) \tag{22}$$

is normal to the contours always pointing away from the ordinate. It is typical of internal gravity waves that the vertical components of the phase and group velocities have different signs.

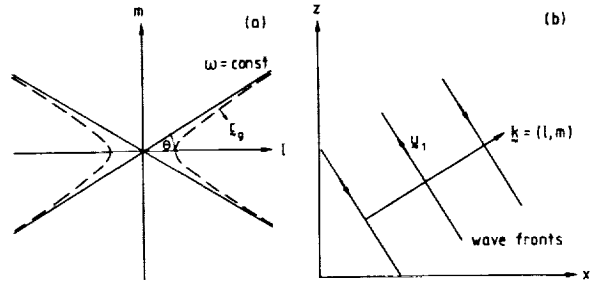

Fig. 1. (a) Contours of constant frequency in the wavenumber domain for internal gravity waves in an incompressible fluid (dashed lines) and in a Boussinesq fluid (continuous lines). The group velocity $\mathbf{c}_g$ is normal to the contours. (b) Internal gravity waves are transverse with the fluid velocity parallel to the wave fronts.

For short wavelengths with $l^2 + m^2 >> 1/4H^2$, (21) yields

$$\omega^2 = N^2 \cos^2 \theta \tag{23}$$

where without loss of generality, θ is the angle between the horizontal and the wavenumber vector $\mathbf{k} = (l, m)$ with $|\theta| \leq \pi/2$. The short wave dispersion equation (23) could have been obtained directly from the equations of motion by applying the Boussinesq approximation which consists of neglecting density variations in the inertia terms but retaining them in the buoyancy term. Then the last term on the left of (11) vanishes and (23) follows immediately. With the Boussinesq approximation, the hyperbolic contours $\omega = \text{const}$ in Figure 1a degenerate to linear asymptots of the hyperbolae including the angle θ with the l axis indicating that this approximation is the better the larger $\mathbf{k}$.

From (9) and (10) we find that plane internal gravity waves are transverse with $\mathbf{u}_1$ in the $x - z$ plane parallel to the wave fronts (Figure 1b). Note that at $\theta = 0$, the phase propagation is horizontal and $\mathbf{u}_1$ vertical, showing that for small vertical displacements and $N^2 > 0$, an air parcel oscillates at the Väisälä-Brunt frequency.

A concise description of further details of the linearized theory of wave propagation such as wave energy, wave action, slowly varying wave trains in nonuniform media etc. is given by BRETHERTON (1971).

We will complete this chapter by showing MST radar observations that indicate the relevance and applicability of the foregoing to dynamic processes in the troposphere, stratosphere and mesosphere. Figure 2 contains contour lines of the power density of vertical velocities observed after the passage of a severe thunderstorm. Convective

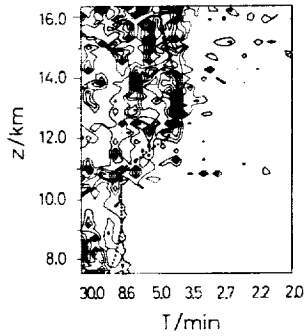

Fig. 2. Time-height contours of power spectra of vertical velocity measured with the SOUSY VHF Radar on 2 June 1978 after the passage of a thunderstorm. The peaks of the spectrogram correspond to a power of $1.1 \times 10^{-5} \mathrm{m^2 s^{-2}}$. The dotted curve represents the height profile of the Väisälä-Brunt period obtained from radiosonde data (from RÖTTGER, 1980).

activity in the troposphere at times of thunderstorms should in particular excite internal wave motions in the stratosphere because rising columns of tropospheric air may penetrate a short distance through the tropopause and transfer kinetic energy to the stably stratified stratosphere (STULL, 1976). The spectrogram in Figure 2 demonstrates that oscillations with periods larger than $2\pi/N$ are observed at all heights with the strongest oscillations occurring above the tropopause at a height near 10 km. No oscillations are found at periods less than $2\pi/N$ so that it appears possible to derive mean potential temperature profiles from the cut-off period of gravity wave spectra (RÖTTGER, 1980).

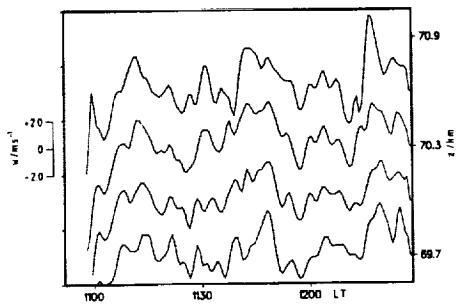

Fig. 3. Time variation of vertical velocity at four heights measured with the mobile SOUSY VHF Radar at Andenes (Norway) on 21 January 1984. Spectral analysis reveals significant peaks at periods near 5, 16 and 30 min (from RÜSTER, 1984).

Figure 3 shows the time dependence of the vertical velocity component of gravity waves measured in the arctic mesosphere. The spectra of the time series have three significant peaks at periods near 5, 16 and 30 min. Spectra with multiple peaks appear to be the rule rather than the exception at mesospheric heights. Almost all radar records show the presence of horizontally propagating waves with periods near $2\pi/N$ that must be generated by local sources rather than sources at lower atmospheric regions. Two possible source mechanism, Kelvin-Helmholtz and parametric instabilities, will be addressed in the next two chapters. There seem to be no detailed case studies of the horizontal and vertical phase propagation of short-period gravity waves in the literature.

3. WAVE-MEAN FLOW INTERACTION

In the previous chapter we discussed linear gravity waves that do not interact. If interaction among waves or between waves and mean flow takes place, we can distinguish between weak and strong interactions. In weak interactions, the space

and time scales of energy exchange processes greatly exceed the typical wavelengths and periods so that the solutions of the equations of motion can be expressed as power series of small nondimensional parameters and can be found by perturbation methods (KEVORKIAN and COLE, 1981). An example will be given in the next chapter. Here we will study two types of strong wave-mean flow interaction characterized by energy exchanges occurring over scales comparable to the wavelength and period. The first type is the critical layer absorption of internal gravity waves loosing their momentum to a vertically sheared mean flow, the second one is the stability of parallel flows to infinitesimal wave perturbations.

3.1. GRAVITY WAVE CRITICAL LEVEL

Besides being partially or totally reflected by a height dependent mean wind $u_0(z)$, an internal gravity wave can meet a critical level $z = z_c$ at which $u_0(z)$ is equal to its horizontal phase speed. In a continuously stratified shear flow, the Richardson number is defined by

$$Ri = \frac{N^2}{u_{0z}^2} \tag{24}$$

representing the ratio of the energy required to interchange vertically adjacent fluid parcels against the gravity acceleration to the available kinetic energy (e.g. CHANDRASEKHAR, 1961). For $Ri > 1/4$, ray theory describing the propagation of waves

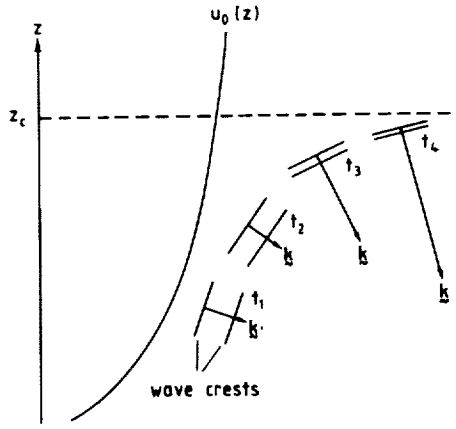

Fig. 4. Schematic of progression of a gravity wave packet propagating toward a critical level z_c at four different times. The horizontal component of **k** remains constant. The fluid velocity is parallel to the wave fronts.

in a slightly nonuniform medium can be used to study how an internal gravity wave packet approaches a critical level (BRETHERTON, 1966). The result is summarized in Figure 4 showing that the wavenumber increases and the perturbation velocity $\mathbf{u}_1$ becomes more and more horizontally oriented as the packet comes closer to z_c. Moreover, the time required for the packet to reach z_c becomes infinite indicating that the packet would be effectively absorbed rather than reflected or transmitted.

Since ray theory becomes invalid at the critical level, the Frobenius method was used to determine the behaviour of an internal gravity wave at z_c (BOOKER and BRETHERTON, 1967). We again describe the perturbed state of the atmosphere by (7) but assume

$$\mathbf{u} = (u_0(z) + u_1, w_1) \tag{25}$$

considering only two-dimensional motions in the $x-z$ plane. Substituting into (1)-(3), neglecting products of perturbation quantities and eliminating ρ_1, p_1 and u_1 yields under the Boussinesq approximation

$$\frac{d^2}{dt^2}(w_{1xx} + w_{1zz}) - \frac{d}{dt}(u_{0zz}w_{1x}) + N^2 w_{1xx} = 0 \tag{26}$$

where $d/dt = \partial/\partial t + u_0\partial/\partial x$. Equation (26) reduces to the Boussinesq approximation of (11) for $u_0 = 0$, and with $N = \text{const}$, $u_0 = \text{const}$ and (12) yields the dispersion relation

$$\Omega^2 = N^2 \cos^2\theta \tag{27}$$

where $\Omega = \omega - lu_0$ is the intrinsic (or Doppler-shifted) frequency. If u_0 is height dependent, there is a new restoring effect due to the vertical derivative of the mean vorticity u_{0z}. Assuming a solution of the form

$$w_1 = W_1(z)e^{il(x-ct)} \tag{28}$$

then gives the Boussinesq form of the Taylor-Goldstein equation

$$(u_0 - c)^2 W_1'' + [N^2 - (u_0 - c)u_0'' - (u_0 - c)^2 l^2]W_1 = 0 \tag{29}$$

with the prime denoting differentiation with respect to z. The original form of the Taylor-Goldstein equation obtained from (1)-(3) without Boussinesq approximation is

$$[\rho_0(u_0 - c)W_1']' - (\rho_0 u_0' W_1)' - \left[\frac{\rho_0' g}{u_0 - c} + \rho_0(u_0 - c)l^2\right] W_1 = 0. \tag{30}$$

Besides containing the important special cases of internal gravity wave propagation and static instability for $u_0 = 0$, (29) is the starting point for analysing the effects of wind shear on gravity waves. For further studies of the critical level problem we note that at $z = z_c, u_0 - c = 0$ so that (29) has a singularity across which solutions have

to be joined. We assume that around $z = z_c, u_0$ and N can be expanded in power series

$$\begin{aligned} u_0 &= c + u_0'(z_c)(z - z_c) + \cdots \\ N &= N(z_c) + N'(z_c)(z - z_c) + \cdots \end{aligned} \tag{31}$$

with $u_0'(z_c) \neq 0$ and try to find a solution of the form

$$W_1 = \sum_{j=0}^{\infty} a_j (z - z_c)^{\alpha + j}, \quad a_0 \neq 0. \tag{32}$$

Substituting (31) and (32) into (29) yields

$$\alpha = \frac{1}{2} \pm i\mu, \quad \mu = (Ri(z_c) - \frac{1}{4})^{\frac{1}{2}} \tag{33}$$

requiring $Ri(z_c) \geq 1/4$ for real μ. Then the general solution near $z = z_c$ is

$$W_1 \approx A(z - z_c)^{\frac{1}{2} + i\mu} + B(z - z_c)^{\frac{1}{2} - i\mu}. \tag{34}$$

The foregoing analysis gives no indication how to join the solutions across $z = z_c$. A proper treatment requires some length (BOOKER and BRETHERTON, 1967) and is therefore beyond the scope of this lecture. One finds that for $u_0'(z_c) > 0$, the A-wave $W_{1A} = A(z - z_c)^{1/2 + i\mu}$ is associated with upward propagating energy for $z < z_c$ and $z > z_c$ whereas the B-wave $W_{1B} = B(z - z_c)^{1/2 - i\mu}$ is associated with downward propagating energy. For $u_0'(z_c) < 0$, the roles of both waves are reversed, and we obtain

$$\begin{aligned} |W_{1A}(z > z_c)| &= |W_{1A}(z < z_c)| e^{-\mu\pi \, \mathrm{sgn} u_0'(z_c)} \\ |W_{1B}(z > z_c)| &= |W_{1B}(z < z_c)| e^{\mu\pi \mathrm{sgn} u_0'(z_c)} \end{aligned} \tag{35}$$

indicating that both waves are severely attenuated as they cross z_c. The vertical flux of horizontal momentum is independent of height on each side of z_c but discontinuous across z_c with the attenuation factor $e^{-2\pi\mu}$ suggesting that there is significant horizontal momentum transfer to the mean flow at the critical level.

From (34) we find that near z_c,

$$|w_1| \sim |z - z_c|^{\frac{1}{2}}, \quad |u_1| \sim |z - z_c|^{-\frac{1}{2}} \tag{36}$$

indicating that w_1 is well behaved whereas u_1 tends to infinity at z_c. The wave-associated shear tends to become infinite at an even higher rate:

$$|u_{1z}| \sim |z - z_c|^{-\frac{3}{2}}. \tag{37}$$

According to BOOKER and BRETHERTON (1967), these infinities are spurious in the sense that nature always generates wave packets of finite spectral width so that all Fourier components with infinitesimal amplitude encounter critical levels at

different heights and the infinities do not in fact occur in the total integrated disturbance. Nevertheless, gravity waves generated by sufficiently monochromatic sources may produce large-amplitude oscillations near critical levels so that one of the hitherto neglected mechanisms may become important: (1) Nonlinearities due to large perturbation amplitudes; (2) molecular dissipation due to strong vertical variations; (3) instability due to strong vertical shears.

3.2 KELVIN-HELMHOLTZ INSTABILITY

For illustrating some of the mechanisms and concepts of dynamic stability, we will work through a classic problem that was first addressed in 1868 by Helmholtz and in 1871 by Kelvin, and demands only little mathematics. We consider a basic flow of an incompressible inviscid two-layer fluid that has unlimited extent, constant densities ρ_I

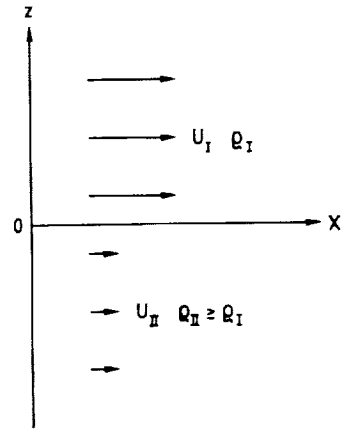

Fig. 5. Kelvin-Helmholtz flow configuration.

and ρ_{II}, and horizontal velocities U_I and U_{II} (Figure 5). We assume that the flow is disturbed by an infinitesimal perturbation displacing the interface between the two layers from $z = 0$ to

$$z = \zeta_1(x, t). \tag{38}$$

Since the model is discontinuous, the Taylor-Goldstein equation (30) must be solved separately in each layer, and both solutions must be matched across the interface $z = \zeta_1$ by two matching conditions.

(1) The interfacial displacement has to be continuous. To first order $w_1(+0) = \zeta_{1t} + U_I\,\zeta_{1x}$ and $w_1(-0) = \zeta_{1t} + U_{II}\zeta_{1x}$ at the upper and lower sides of the interface, respectively. For a travelling wave solution of the form (28) we then get

C-4

$$\frac{w_1(+0)}{U_I - c} = \frac{w_1(-0)}{U_{II} - c}. \tag{39}$$

(2) At $z = \zeta_1$, the total pressure must be continuous. Using Bernoulli's theorem (e.g. LAMB, 1945), we obtain

$$\rho_I \left[(U_I - c)w_1'(+0) - \frac{g}{U_I - c} w_1(+0)\right] = \rho_{II} \left[(U_{II} - c)w_1'(-0) - \frac{g}{U_{II} - c} w_1(-0)\right]. \tag{40}$$

The perturbation is further assumed to decay to zero for $|z| \to \infty$ yielding the boundary conditions

$$w_1 \to 0 \text{ as } z \to \pm\infty. \tag{41}$$

For the Kelvin-Helmholtz flow configuration (Figure 5), the Taylor-Goldstein equation (30) reduces to

$$W_1'' - l^2 W_1 = 0 \tag{42}$$

and must have a solution of the form

$$W_1 = \begin{cases} Ae^{-lz} & \text{at } z > 0 \\ Be^{lz} & \text{at } z < 0 \end{cases} \tag{43}$$

to satisfy the boundary conditions (41). Equations (39) and (40) then yield two homogeneous linear equations for A and B which are nontrivial only if

$$c = \frac{\rho_{II} U_{II} + \rho_I U_I}{\rho_{II} + \rho_I} \pm \left[\frac{\rho_{II} - \rho_I}{\rho_{II} + \rho_I} \frac{g}{l} - \frac{\rho_{II}\rho_I}{(\rho_{II} + \rho_I)^2}(U_{II} - U_I)^2\right]^{\frac{1}{2}} \tag{44}$$

The first term on the right of (44) may be considered as the density-weighted mean velocity of the two fluid layers. The wave perturbation then travels with a velocity d given by

$$d^2 = d_0^2 - \frac{\rho_{II}\rho_I}{(\rho_{II} + \rho_I)^2}(U_{II} - U_I)^2 \tag{45}$$

relative to the mean velocity where

$$d_0 = \left(\frac{\rho_{II} - \rho_I}{\rho_{II} + \rho_I} \frac{g}{l}\right)^{\frac{1}{2}} \tag{46}$$

is the phase velocity in the absence of any basic flow. For

$$(U_{II} - U_I)^2 > \frac{\rho_{II}^2 - \rho_I^2}{\rho_{II}\rho_I} \frac{g}{l} \tag{47}$$

c is complex so that the wave perturbation grows and remains stationary with respect to the mean flow. For any given $U_{II} - U_I \neq 0$, the interface is unstable for sufficiently

small wavelengths. If $\rho_{II} = \rho_I$, it is unstable for all wavelengths indicating the stabilizing influence of a density change. Finally we note that for small density changes, $\rho_{II}^2 - \rho_I^2 \approx 2\rho_{II}(\rho_{II} - \rho_I)$. Then we can define a Richardson number by

$$Ri = \frac{\rho_{II} - \rho_I}{\rho_I (U_{II} - U_I)^2} \frac{g}{l} \tag{48}$$

so that $Ri > \frac{1}{2}$ ($< \frac{1}{2}$) for stability (instability).

The instability of the Kelvin-Helmholtz flow configuration at high wavenumbers is a consequence of the fact that vorticity is concentrated at a single height. A physically more realistic model together with the neutral stability curve obtained by DRAZIN (1958) is shown in Figure 6, where

$$u_0 = \Delta u \tanh(\frac{z}{d}), \quad \rho_0 = e^{-\frac{N^2 z}{g}}, \quad Ri = \left(\frac{Nd}{\Delta u}\right)^2 \tag{49}$$

The flow is stable for $Ri > 1/4$. We note that the expression "Kelvin-Helmholtz instability" is also used for shear flow instability in models with continuous density and wind profiles.

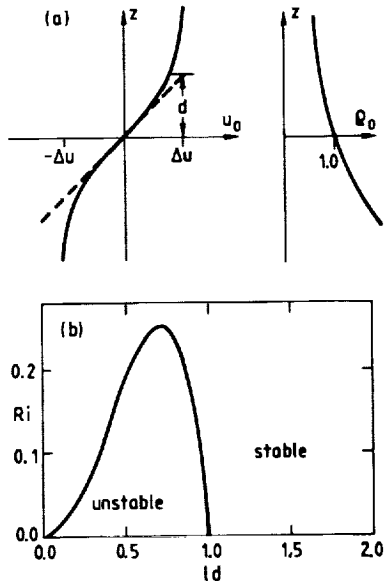

Fig. 6. (a) DRAZIN's (1958) model. (b) Neutral stability curve.

We conclude the theoretical part of this chapter by summarizing some general results on the stability of nonrotating stratified shear flows (for details cf. LE BLOND

and MYSAK (1978)).

(1) YIH's (1955) extension of SQUIRE's (1933) theorem: For each unstable three-dimensional disturbance in a stratified fluid, there is a more unstable two-dimensional one propagating parallel to the flow. For this reason we have considered only two-dimensional waves of the form (28).

(2) SYNGE's (1933) theorem: A necessary condition for instability is

$$[(U - c_r)^2 + c_i^2](\rho_0 U')' - 2(U - c_r)\rho_0 N^2 = 0 \tag{50}$$

somewhere in the field of flow. Here, $c_r = \mathrm{Re}c$ and $c_i = \mathrm{Im}c$. For $\rho_0 = \text{const}$, (50) yields $U'' = 0$ which is Rayleigh's inflection point theorem.

(3) MILES' (1961) stability condition: A sufficient condition for stability is $Ri \geq 1/4$ everywhere in the flow.

(4) HOWARD's (1961) semicircle theorem: The complex wave velocity c of an unstable wave with $c_i > 0$ lies in the semicircle

$$[c_r - (u_{0\max} + u_{0\min})/2]^2 + c_i^2 \leq [(u_{0\max} - u_{0\min})/2]^2. \tag{51}$$

There are characteristic streamline patterns of fluid motions near critical levels known as cat's eyes. For $N = 0$ and $u_o - c \sim z - z_c$, Kelvin derived from (29) the cat's eye pattern shown in Figure 7a as seen by an observer moving with the wave velocity. The existence of closed streamline patterns is a purely kinematic consequence of a finite vertical velocity component at the critical level. In a stratified flow ($N > 0$), the cat's eye pattern becomes asymmetric as indicated by Taylor's cockeyed cat's eye in a three-layer model fluid (Figure 7b). According to HOWARD and MASLOWE (1973), also intermediate forms between Kelvin's and Taylor's cat's eye patterns are possible.

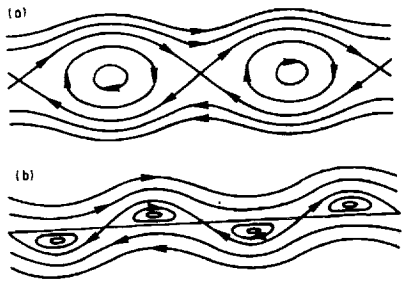

Fig. 7. (a) Kelvin's cat's eye streamline pattern. (b) Taylor's cockeyed cat's eye streamline pattern.

There is evidence that cat's eye structures occur in the time-height distributions of MST radar echo power both in the troposphere (RÖTTGER and SCHMIDT, 1979)

and in the mesosphere (REID et al., 1987) (Figures 8 and 9). The enhanced echo power is probably due to enhanced turbulence in thin layers surrounding the regions of closed streamlines (KELLY and MASLOWE, 1970).

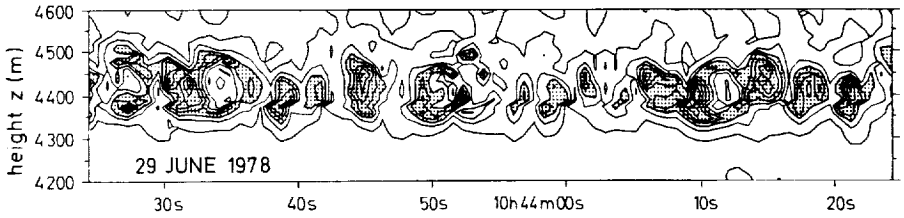

Fig. 8. Contour plot of constant MST radar echo power in the time-height plane indicating cat's eye structures (from RÖTTGER and SCHMIDT, 1979).

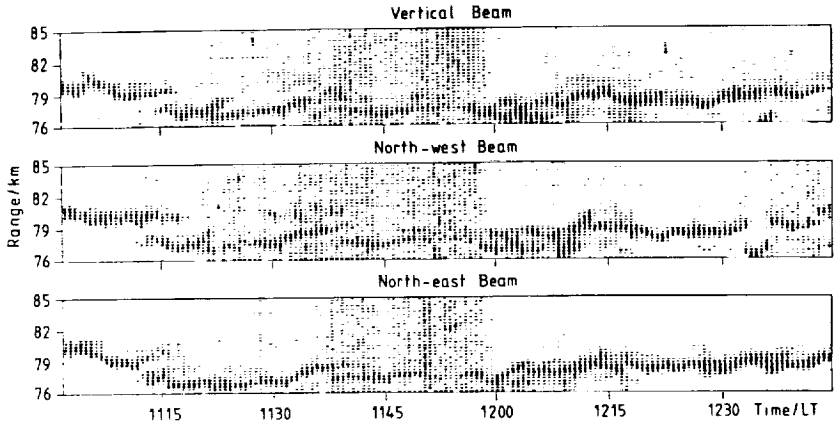

Fig. 9. Time-height intensity plot of MST radar echo power in three antenna beam directions. A cat's eye is visible between 11:55 and 12:10 LT (from REID et al., 1987).

Detailed investigations of cat's eye patterns observed by MST radars have not yet been performed, but there are three examples of Kelvin-Helmholtz instabilities that were analyzed and compared to numerical model computations (VANZANDT et al., 1979; KLOSTERMEYER and RÜSTER, 1980, 1981; RÜSTER and KLOSTERMEYER, 1983). Figure 10 shows the radial velocity oscillations associated with a Kelvin-Helmholtz instability at the bottom side of a polar jetstream and measured

with height and time resolutions of 150 m and 10 s, respectively. The oscillations reveal a period of about 4 min and amplitudes of the order of 1 m s^{-1}. The critical level

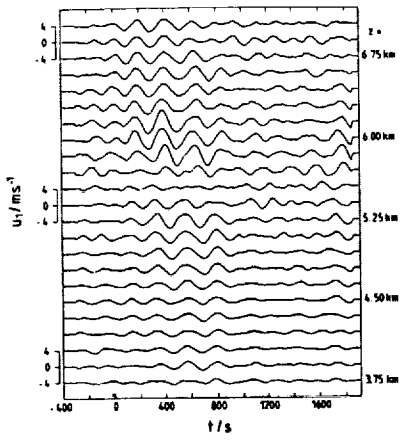

Fig. 10. Band pass-filtered time series of radial velocity oscillations associated with a Kelvin-Helmholtz instability and measured by the SOUSY VHF Radar on 11 April 1980 (from KLOSTERMEYER and RÜSTER, 1981).

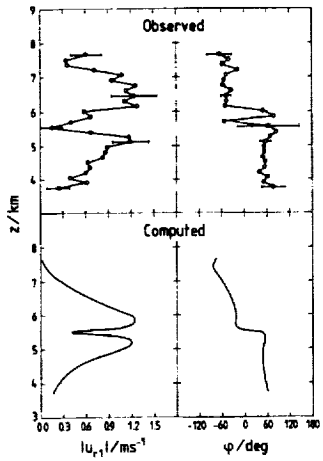

Fig. 11. Measured and computed height profiles of Kelvin-Helmholtz-associated velocity oscillations (from KLOSTERMEYER and RÜSTER, 1980).

is near $z = 5.55$ km and is indicated by a vanishing amplitude and a sudden phase jump of about 100°. Figure 11 shows a comparison between measured and computed height profiles of the amplitude and phase of the radial velocity oscillations. Further studies indicate that the growth of the observed Kelvin-Helmholtz instability is limited by the onset of static instability producing periodic radar echo power bursts (KLOSTERMEYER and RÜSTER, 1981).

4. WAVE-WAVE INTERACTION

Here we will investigate the general nature of weak resonant interaction between wave triplets and will always keep in mind that this is an oversimplification of natural processes which consist of resonant and forced energy transfer over continuous wavenumber and frequency domains. The actual wave spectrum thus is the result of a balance between the effects of sources, dissipation and redistribution due to nonlinear interaction. Moreover, the application of a weakly nonlinear theory which is based on perturbation methods, is restricted to small-amplitude waves. It should be mentioned, however, that the stability of a monochromatic internal gravity wave with arbitrary amplitude is closely related to weak resonant interactions. This so-called parametric instability provides a simple example for the instability of time dependent and spatially varying flows and will therefore be discussed in the second part of this chapter.

4.1. WEAK WAVE-WAVE INTERACTION

If we take into account the nonlinear terms that have been neglected in the previous chapters, we obtain a wave equation of the form

$$\mathcal{L}(w) + \mathcal{Q}(w, w) = 0 \tag{52}$$

where $\mathcal{L}$ and $\mathcal{Q}$ are differential operators which are linear and quadratic in w, respectively, and w represents any of the perturbation variables. We assume that there is a small nondimensional quantity ε characterizing the relative magnitude of the nonlinear term in (52). In a straight-forward perturbation procedure we expand w in powers of ε,

$$w = \varepsilon w_1 + \varepsilon^2 w_2 + \ldots \tag{53}$$

and solve the equations

$$\mathcal{L}(w_1) = 0, \tag{54}$$

$$\mathcal{L}(w_2) = -\mathcal{Q}(w_1, w_1) \text{ etc.} \tag{55}$$

Provided the expansion (53) converges we thus obtain a solution for (53) for waves of finite but small amplitudes (for details of perturbation methods cf. KEVORKIAN

and COLE (1981)). According to Chapter 2, (54) yields plane wave solutions in uniform atmospheric models so that

$$w_1 = \frac{1}{2} W_1 e^{i\mathbf{k}\cdot\mathbf{r}-\omega t} + \text{complex conjugate} \tag{56}$$

where the wavenumber vector $\mathbf{k}$ and angular frequency ω satisfy a dispersion relation

$$\mathcal{D}(\mathbf{k},\omega) = 0. \tag{57}$$

To second order in ε we get from (55) a nonhomogeneous linear equation for w_2 with a forcing term depending on w_1. The process can be continued to any order of ε.

Now we consider the case that w_1 consists of two plane waves,

$$w_1 = w_a + w_b \tag{58}$$

both satisfying (54) and (57). Then (55) becomes

$$L(w_c) = -\mathcal{Q}(w_a + w_b, w_a + w_b) \tag{59}$$

where $w_2 = w_c$ is the result of the interaction between w_a and w_b. Since the quadratic operator on the right of (59) produces plane waves with wavenumber vectors $\mathbf{k}_c = 0,\ \pm 2\mathbf{k}_a,\ \pm 2\mathbf{k}_b,\ \pm(\mathbf{k}_a \pm \mathbf{k}_b)$ and corresponding angular frequencies ω_c, w_c has the form

$$w_c = \frac{1}{2} \sum \frac{W_c e^{i(\mathbf{k}_c\cdot\mathbf{r}-\omega_c t)} + \text{complex conjugate}}{\mathcal{D}(\mathbf{k}_c,\omega_c)} \tag{60}$$

provided $\mathcal{D}(\mathbf{k}_c,\omega_c) \neq 0$. The summation is performed over all sign combinations resulting from the quadratic forcing term in (59). If $a = b$ and both signs are allowed for all wavenumbers and frequencies, all cases can be described by

$$\mathbf{k}_a + \mathbf{k}_b + \mathbf{k}_c = 0,\ \omega_a + \omega_b + \omega_c = 0. \tag{61}$$

The forced wave $\varepsilon^2 w_c$ plays only a minor role in (53) as compared to $\varepsilon(w_a + w_b)$ unless $\mathcal{D}(\mathbf{k}_c,\omega_c) = 0$. Then resonance occurs so that the amplitude of w_c grows in space and time. Such a resonant wave is also called secular. It dominates the non-resonant waves after the interaction has lasted for some time and can therefore be considered as the most significant result.

It depends on the specific form of the dispersion relation whether three interacting waves can satisfy the resonance conditions (61) and (57). Clearly, if the waves are nondispersive, i.e. propagate at the same speed, all interactions are resonant. For internal gravity waves in a Boussinesq fluid with $N = \text{const}$, the resonance conditions may be written

$$\mathbf{k}_a \pm \mathbf{k}_b = \mathbf{k}_c,\ \cos\theta_a \pm \cos\theta_b = \cos\theta_c \tag{62}$$

using (23). The loci of resonant triads can be calculated from simple geometrical considerations and are shown in Figure 12. It should be mentioned, however, that the Boussinesq approximation consists of neglecting terms of first and higher orders in the ratio of wavelength to density scale height (Chapter 2) and thus is only applicable if this ratio is much smaller than ε (LONG, 1965).

YEH and LIU (1985) pointed out that resonant wave interaction may play an important role in the evolution of the atmospheric wave spectrum. There are in particular three classes of resonant triads that can provide efficient energy transfer between separate parts of the gravity wave spectrum and have first been identified by MCCOMAS and BRETHERTON (1977) as elastic scattering, induced diffusion and parametric subharmonic instability (Figure 13). By elastic scattering, an upgoing

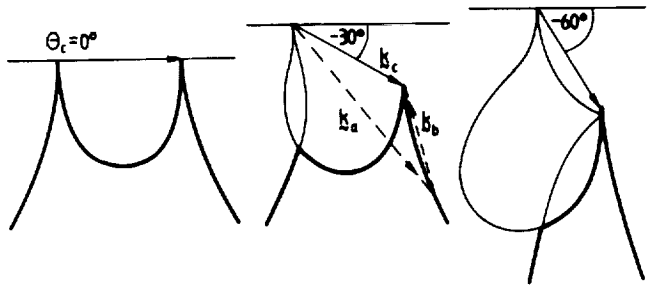

Fig. 12. Resonant interaction diagrams for internal gravity waves in a Boussinesq fluid for $\theta_c = 0°, -30°$ and $-60°$. Any point on a branch defines a resonant triad satisfying (62). The wavenumber vector with the least slope is always the vector sum of the other two. Thick (thin) branches indicate unstable (stable) triads (after PHILLIPS, 1969).

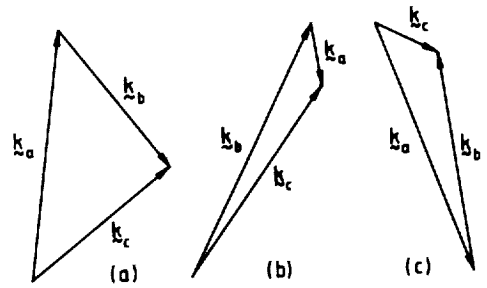

Fig. 13. Characteristic classes of resonant triads:
(a) elastic scattering, (b) induced diffusion, (c) parametric subharmonic instability.

wave is scattered into a downgoing one by resonantly interacting with a low frequency, nearly vertically propagating wave with almost twice the vertical wavenumber of the other two waves. This process makes the atmospheric spectrum vertically symmetric if it is not so initially. The process of induced diffusion is responsible for the evolution of small-scale waves and consists of two almost identical waves which interact resonantly with a large-scale low-frequency wave propagating almost vertically. Finally, in the process of parametric subharmonic instability, two waves with nearly opposite large wavenumber vectors and almost identical frequencies resonate with a third wave having a much smaller wavenumber and twice the frequency. This mechanism provides energy transfer from an energetic large-scale wave to small-scale waves at subharmonic frequencies.

4.2. PARAMETRIC INSTABILITY

There is a close connection between the interaction of weak internal gravity waves and the parametric instability of a monochromatic internal gravity wave of arbitrary amplitude (MIED, 1976; KLOSTERMEYER, 1982, 1983). For studying parametric instability, it is useful to assume a uniformly stratified Boussinesq model and to introduce the stream function Ψ which describes the two-dimensional motion of an incompressible fluid in the $x - z$ plane by

$$\mathbf{u} = (\Psi_z, -\Psi_x) \tag{63}$$

and satisfies (2). We further introduce the buoyancy

$$B = -\frac{\rho - \rho_*}{\rho_*} g \tag{64}$$

where ρ_* is some suitable constant reference density used in the Boussinesq approximation to replace ρ in the inertia terms (e.g. LEBLOND and MYSAK, 1978). Buoyancy and Väisälä-Brunt frequency are related by

$$N^2 = B_z. \tag{65}$$

Equations (3) and (1) then yield

$$\nabla^2 \Psi_t + B_x = \Psi_x \nabla^2 \Psi_z - \Psi_z \nabla^2 \Psi_x \tag{66}$$

$$B_t - N^2 \Psi_x = \Psi_x B_z - \Psi_z B_x \tag{67}$$

We note that (66) results from the vorticity equation that is obtained by taking the curl of (3). The plane wave

$$\Psi = A \cos \varphi, \quad B = -N^2 l \omega^{-1} A \cos \varphi \tag{68}$$

with $\varphi = lx + mz - \omega t$ is a solution of (66) and (67) if the dispersion relation (23) is satisfied. The nonlinear terms are identically zero as a consequence of incompressibility.

We thus have the opportunity to investigate the stability of a finite-amplitude plane internal gravity wave by expressing the stream function and buoyancy fields as sums of the basic state (68) and a perturbation:

$$\Psi = A\cos\varphi + \psi, \quad B = -N^2 l\omega^{-1} A\cos\varphi + b. \tag{69}$$

We define nondimensional variables by

$$(\tilde{x}, \tilde{z}) = k(x, z), \ \tilde{t} = Nt, \ \tilde{\Psi} = k^2 N^{-1}\Psi, \ \tilde{B} = kN^{-2}B, \ M = k^2(2N)^{-1}A \tag{70}$$

with $k = (l^2 + m^2)^{1/2}$ and introduce a rotated coordinate system (ξ, η) such that the η axis coincides with the direction of propagation of the basic wave (Figure 14).

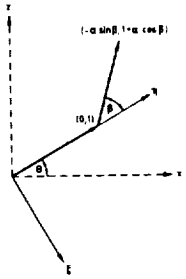

Fig. 14. Wavenumber vector of basic internal gravity wave, (0,1), and Floquet vector $(-\alpha\sin\beta, \alpha\cos\beta)$ in $\xi - \eta$ coordinates (from KLOSTERMEYER, 1982).

Substituting (69) into (66) and (67) and neglecting terms containing products of the perturbation quantities ψ and b then yields

$$\begin{aligned} \nabla^2\psi_t &+ \sin\theta b_\xi + \cos\theta b_\eta = 2M\sin\varphi(\psi_\xi + \nabla^2\psi_\xi) \\ b_t &- \sin\theta\psi_\xi - \cos\theta\psi_\eta = 2M\sin\varphi(\psi_\xi + b_\xi) \end{aligned} \tag{71}$$

where the tilde of the nondimensional variables has been omitted and $\nabla^2 = \partial^2/\partial\xi^2 + \partial^2/\partial\eta^2, \varphi = \eta - \cos\theta t$. The terms on the right of (71) couple the perturbations with

the basic state via a periodic coefficient $2M\sin\varphi$ so that ψ and b take a parametric form dictated by Floquet theory (MIED, 1976):

$$(\psi, b) = e^{i(-\alpha\sin\beta\xi+\alpha\cos\beta\eta)+\lambda t}\sum_{j=-\infty}^{\infty}(\psi_j, b_j)e^{ij\varphi}. \tag{72}$$

As indicated in Figure 14, $|\alpha|$ can be considered as the magnitude of a Floquet vector forming an angle β with the basic wavenumber vector. Substitution of (72) into (71) yields a linear eigenvalue problem for the complex quantities λ and (ψ_j, b_j),

$$\begin{aligned} p_j^{(-1)}\psi_{j-1} &+ (p_j^{(0)}-\lambda)\psi_j + q_j^{(0)}b_j + p_j^{(1)}\psi_{j+1} = 0 \\ r_j^{(-1)}\psi_{j-1} &+ s_j^{(-1)}b_{j-1} + r_j^{(0)}\psi_j + (s_j^{(0)}-\lambda)b_j + r_j^{(1)}\psi_{j+1} + s_j^{(1)}b_{j+1} = 0 \end{aligned} \tag{73}$$

with $j = 0, \pm1, \pm2...$ and constant coefficients p, q, r, s depending on $j, M, \theta, \alpha, \beta$ (cf. KLOSTERMEYER, 1982). Solutions can be obtained numerically for any given accuracy if the interation equations (73) are truncated at $j = \pm J$ with J sufficiently large.

The numerical search for growing disturbances ($\mathrm{Re}\lambda > 0$) is greatly facilitated by considering the case $M \to 0$. Then (73) yields for nontrivial solutions (ψ_j, b_j)

$$\mathrm{Re}\lambda = 0,\ j\cos\theta - \mathrm{Im}\lambda = \frac{\alpha\cos(\theta+\beta)+j\cos\theta}{[(\alpha\sin\beta)^2+(\alpha\cos\beta+j)^2]^{1/2}}. \tag{74}$$

From (72) and Figure 14, the nondimensional perturbation frequencies and wavenumbers in $x-z$ coordinates are

$$\begin{aligned} \omega_j &= j\cos\theta - \mathrm{Im}\lambda \\ \mathbf{k}_j &= (\alpha\cos(\theta+\beta)+j\cos\theta, \alpha\sin(\theta+\beta)+j\sin\theta) \end{aligned} \tag{75}$$

so that with (74)

$$\omega_j = \cos\theta_j \tag{76}$$

where θ_j is the angle between $\mathbf{k}_j$ and the horizontal. For $M \to 0$, the disturbances thus are freely propagating waves that satisfy the resonance conditions

$$\mathbf{k}_{j+1} - \mathbf{k}_j = \mathbf{k},\ \ \omega_{j+1} - \omega_j = \omega \tag{77}$$

for all j. Computations for $M > 0$ show in agreement with HASSELMANN's (1967) criterion for nonlinear wave stability that $\mathrm{Re}\lambda > 0$ (i.e. instability) for resonant sum interactions and $\mathrm{Re}\lambda = 0$ (i.e. stability) for resonant difference interactions. In Figure 12, the loci of unstable triads are indicated by the thick branches.

In a laboratory experiment, DAVIS and ACRIVOS (1967) demonstrated that an internal gravity wave propagating along a diffuse stratified interface between fluids of

different densities may become distorted by the growth of a three-wave resonance giving rise to local turbulent mixing. Their photographs are shown in Figure 15. MCEWAN and ROBINSON (1975) found good agreement between predicted and observed small-scale parametric instabilities in a cylindrical chamber. Although the potential

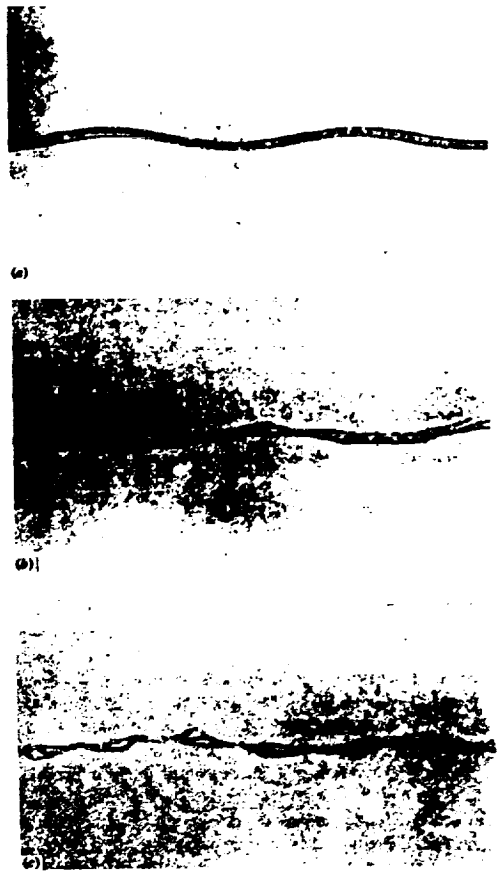

Fig. 15. Progressive distortion of an internal gravity wave by resonant wave-wave interaction (from DAVIS and ACRIVOS, 1967).

role of parametric instability in forming internal wave spectra in the atmosphere has been stressed by some authors (MCEWAN and ROBINSON, 1975; DRAZIN, 1977), there are only few atmospheric observations that have been interpreted in terms of resonant triads or parametric instability. Thus the power spectrum of a strong internal

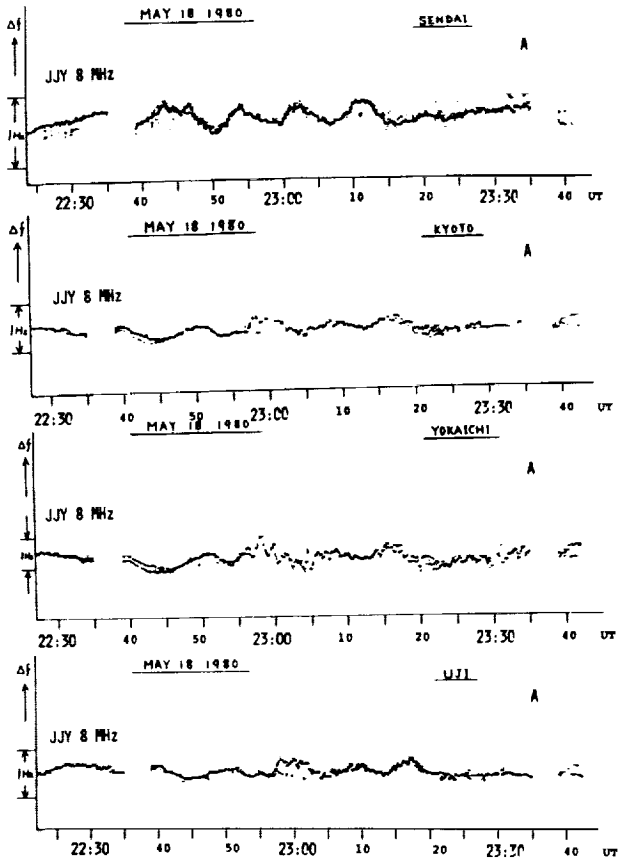

Fig. 16. Doppler shift of a 8 MHz continuous radio wave recorded at four Japanese stations after the eruption of Mount St. Helens on 18 May 1980. In the lower three records, an internal gravity wave with a period near the local Väsisälä-Brunt period is strongly disturbed by short-period oscillations after 22:55 UT (from LIU et al., 1982).

gravity wave in the lower thermosphere which was generated by an eruption of Mount St. Helens, was explained in terms of parametric instability (KLOSTERMEYER, 1984). Figure 16 showing the Doppler shift of an 8 MHz radio wave reflected from the ionosphere near 200 km height, indicates strong high-frequency disturbances superposed on a gravity wave at Kyoto, Yokaichi and Uji after 2255 UT. Note a certain

resemblence of these records to Figure 15c.

RÖTTGER (1987) has noted that time series of spectra intensity plots obtained from MST radar measurements also show high-frequency oscillations superposed on low-frequency gravity waves. An example is seen in Figure 17 at 69.6 km after 1300 AST. Röttger further points out that the amplitude the low-frequency waves does not grow with inreasing height (visible between 1200 and 1300 AST in the height

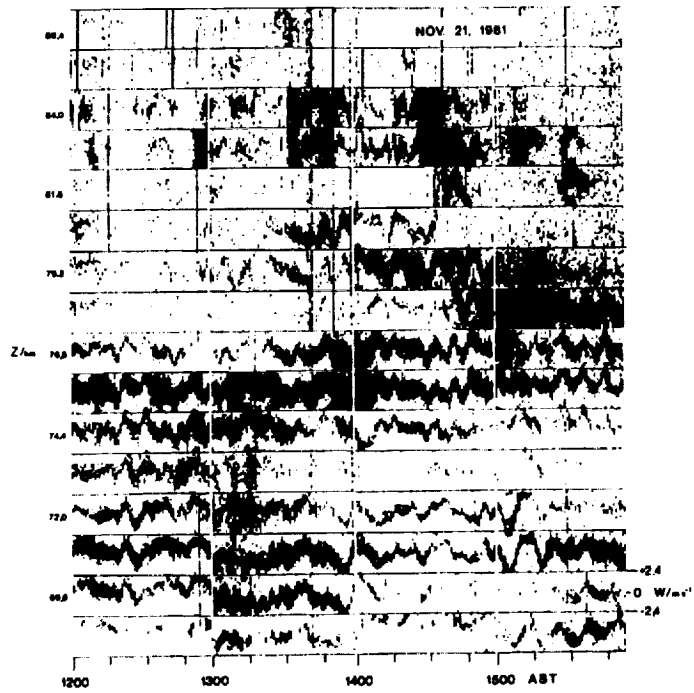

Fig. 17. Time series of spectra intensity plots measured with the mobile SOUSY VHF Radar at the Arecibo Observatory (from RÖTTGER, 1987).

interval from 69.6 to 76.8 km). Since wave breaking discernible from strong echo intensities does not occur some other saturation process such as parametric instability must be considered.

Short-period gravity waves with frequencies close to the local Väisälä-Brunt frequency occur frequently in mesospheric MST radar observations of vertical or near vertical radial velocities (HARPER and WOODMAN, 1976; MILLER et al., 1978).

These waves do not show any vertical phase variation over height intervals of several kilometers indicating that they propagate horizontally and are generated in situ rather than in lower or higher atmospheric regions. Occasionally the local source mechanism is Kelvin-Helmholtz instability of a wind shear due to long-period inertial or tidal waves (KLOSTERMEYER and RÜSTER, 1984; YAMAMOTO et al., 1988). But in general the simultaneously observed wind shear is too weak for Kelvin-Helmholtz instability to set in. A numerical simulation of the wave motions shown in Figure 3 indicates that parametric instability could be another source candidate of the observed short-period waves. Figure 18a shows the same observations as Figure 3 but with very high-frequency noise and high-frequency waves removed by recursive Butterworth filters (continuous and dashed curves respectively). Figure 18b shows the numerical simulation where the dashed lines represent the finite-amplitude basic wave and the continuous lines the sum of the basic wave and the fastest growing parametric instability mode. Note that the height interval in Figure 18b is 75% of the basic vertical wavelength whereas in Figure 18a, it is only about 10%. The observed and computed short-period oscillations show good qualitative agreement. Both reveal in particular considerable temporal amplitude modulation, and the dominating period is not an integer multiple of the basic period. There is in general also no vertical phase variation. But the computed short-period oscillations show sudden phase reversals, e.g. at $Nt = 20$ and $kz = 4.8$. The loci of sudden phase reversals lie on basic wave

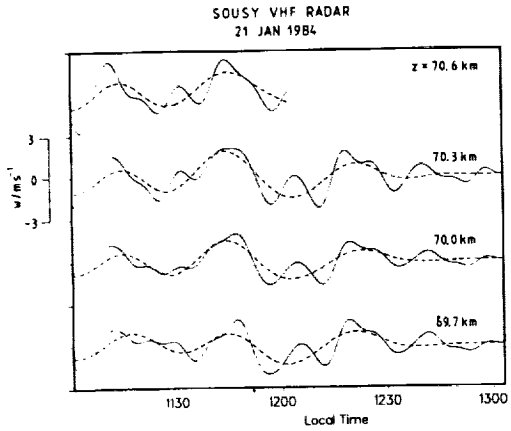

Fig. 18a. Same as Figure 3 but with noise and high-frequency waves removed (continuous and dashed curves, respectively). The time series at z = 70.6 km is not continued beyond 12 LT with regard to very small signal-to-noise ratios.

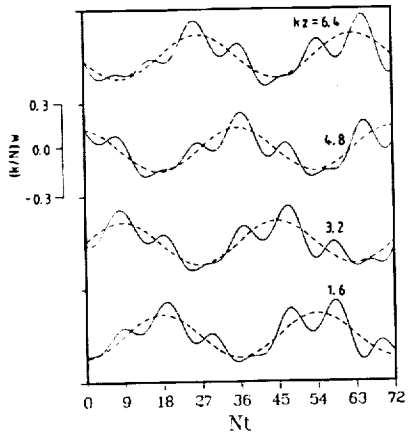

Fig. 18b. Numerical simulation of a parametric instability. The dashed and continuous lines represent the basic wave and the sum of basic wave and fastest growing instability mode, respectively. Time, height and vertical velocity component are normalized according to (70).

fronts. Whereas there is no clear evidence for phase reversals in Figure 18a (perhaps due to the small height interval) they become visible if velocity measurements can be obtained over larger height intervals (e.g. Figure 1 of MILLER et al. (1978)).

Acknowledgement. I thank Dr. Bernd Inhester for valuable comments and Mrs. Karin Peschke for carefully typing the manuscript.

REFERENCES

Booker, J.R., and F.P. Bretherton, The critical layer for internal gravity waves in a shear flow, *J. Fluid Mech.*, **27**, 513-539, 1967.

Bretherton, F.P., The propagation of groups of internal gravity waves in a shear flow, *Q.J.R. Meteorol. Soc.*, **92**, 466-480, 1966.

Bretherton, F.P., The general linearized theory of wave propagation, In: *Mathematical Problems in the Geophysical Sciences* (W.H. Reid, ed.), 61-102, Am. Math. Soc., Providence, Rhode Island, 1971.

Chandrasekhar, S., *Hydrodynamic and Hydrodmagnetic Stability*, Clarendon, Oxford, 1961.

Davis, R.E., and A. Acrivos, The stability of oscillatory internal waves, *J. Fluid Mech.*, **30**, 723-736, 1967.

Drazin, P.G., The stability of a shear layer in an unbounded heterogeneous inviscid fluid, *J. Fluid Mech.*, **4**, 214-224, 1958.

Drazin, P.G., On the instability of an internal gravity wave, *Proc. R. Soc. Lond.*, **A356**, 411-432, 1977.

Eckart, C., *Hydrodynamics of Oceans and Atmospheres*, Pergamon, Oxford, 1960.

Harper, R.M., and R.F. Woodman, Preliminary multiheight radar observations of waves and winds in the mesosphere over Jicamarca, *J. Atmos. Terr. Phys.*, **39**, 959-961, 1977.

Hasselmann, K.. A criterion for nonlinear wave stability, *J. Fluid Mech.*, **30**, 737-739, 1967.

Howard, L.N., Note on a paper of John W. Miles, *J. Fluid Mech.*, **10**, 509-512, 1961.

Howard, L.N., and S.A. Maslowe, Stability of stratified shear flow, *Boundary-Layer Meteorol.*, **4**, 511-523, 1973.

Kelly, R.E., and S.A. Maslowe, The nonlinear critical layer in a slightly stratified shear flow, *Stud. Appl. Math.*, **49**, 301-326, 1970.

Kevorkian, J., and J.D. Cole, *Perturbation Methods in Applied Mathematics*, Springer, Berlin, 1981.

Klostermeyer, J., Lamb waves originating in nongeostrophic disturbances: A case study, *J. Geophys. Res.*, **82**, 1441-1448, 1977.

Klostermeyer, J., On parametric instabilities of finite-amplitude internal gravity waves, *J. Fluid Mech.*, **119**, 367-377, 1982.

Klostermeyer, J., Parametric instabilities of internal gravity waves in Boussinesq fluids with large Reynolds numbers, *Geophys. Astrophys. Fluid Dyn.*, **26**, 85-105, 1983.

Klostermeyer, J., Observations indicating parametric instabilities in internal gravity waves at thermospheric heights, *Geophys. Astrophys. Fluid Dyn.*, **29**, 117-138, 1984.

Klostermeyer, J., and R. Rüster, Radar observation and model computation of a jet stream-generated Kelvin-Helmholtz instability, *J. Geophys. Res.*, **85**, 2841-2846, 1980.

Klostermeyer, J., and R. Rüster, Further study of a jet stream-generated Kelvin-Helmholtz instability, *J. Geophys. Res.*, **86**, 6631-6637, 1981.

Klostermeyer, J., and R. Rüster, VHF radar observation of wave instability and turbulence in the mesosphere, *Adv. Space Res.*, **4**, 79-82, 1984.

Lamb, H., *Hydrodynamics*, 6th ed., Dover, New York, 1945.

LeBlond, P.H., and L.A. Mysak, *Waves in the Ocean*, Elsevier, Amsterdam, 1978.

Liu, C.H., J. Klostermeyer, K.C. Yeh, T.B. Jones, T. Robinson, O. Holt, R. Leitinger, T. Ogawa, K. Sinno, S. Kato, T. Ogawa, A.J. Bedard, and L. Kersley, Global dynamic response of the atmosphere to the eruption of Mount St. Helens on May 18, 1980, *J. Geophys. Res.*, **87**, 6281-6290, 1982.

Long, R.R., On the Boussinesq approximation and its role in the theory of internal waves, *Tellus*, **17**, 46-52, 1965.

McComas, C.H., and F.P. Bretherton, Resonant interaction of oceanic internal waves, *J. Geophys. Res.*, **82**, 1397-1412, 1977.

McEwan, A.D., and R.M. Robinson, Parametric instability of internal gravity waves, *J. Fluid Mech.*, **67**, 667-687, 1975.

Mied, R.P., The occurrence of parametric instabilities in finite-amplitude internal gravity waves, *J. Fluid Mech.*, **78**, 763-784, 1976.

Miles, J.W., On the stability of heterogeneous shear flows, *J. Fluid Mech.*, **10**, 496-508, 1961.

Miller, K.L., S.A. Bowhill, K.P. Gibbs, and I.D. Countryman, First measurements of mesospheric vertical velocities by VHF radar at temperate latitudes, *Geophys. Res. Lett.*, **5**, 939-942, 1978.

Phillips, O.M., *The Dynamics of the Upper Ocean*, University Press, Cambridge, 1969.

Reid, I. M., R. Rüster and G. Schmidt, VHF radar observations of cat's-eye-like structures at mesospheric heights, *Nature*, **327**, 43-45, 1987.

Röttger, J., Structure and dynamics of the stratosphere and mesosphere revealed by VHF radar investigations, *Pure Appl. Geophys.*, **118**, 494-527, 1980.

Röttger, J., The relation of gravity waves and turbulence in the mesosphere, *Adv. Space Res.*, **7**, 10345-10348, 1987.

Röttger, J., and G. Schmidt, High-resolution VHF radar sounding of the troposphere and stratosphere, *IEEE Trans. Geosci. Electron.*, **GE-17**, 182-189, 1979.

Rüster, R., Winds and waves in the middle atmosphere as observed by ground based radars, *Adv. Space Res.*, 4, 3-18, 1984.

Rüster, R., and J. Klostermeyer, VHF radar observations of a Kelvin-Helmholtz instability in a subtropical jet stream, *Geophys. Astrophys. Fluid Dyn.*, **26**, 107-116, 1983.

Squire, H.B., On the stability of three-dimensional disturbances of viscous flow between parallel walls, *Proc. R. Soc. Lond.*, **A142**, 621-628, 1933.

Stull, R.B., Internal gravity waves generated by penetrative convection, *J. Atmos. Sci.*, **33**, 1279-1286, 1976.

Synge, J.L., The stability of heterogeneous liquids, *Trans. R. Soc. Can.*, **27(III)**, 1-18, 1933.

VanZandt, T.E., A universal spectrum of buoyancy waves in the atmopshere, *Geophys. Res. Lett.*, **9**, 575-578, 1982.

VanZandt, T.E., J.L. Green, W.L. Clark, and J.R. Grant, Buoyancy waves in the troposphere: Doppler radar observations and a theoretical model, *Geophys. Res. Lett.*, **6**, 429-432, 1979.

Volland, H., The upper atmosphere as a multiply refractive medium for neutral air motions, *J. Atmos. Terr. Phys.*, **31**, 491-514, 1969.

Yamamoto, M., T. Tsuda, S. Kato, T. Sato, and S. Fukao, Interpretation of the structure of mesospheric turbulence layers in terms of inertia gravity waves, *Physica Scripta*, **37**, 645-650, 1988.

Yeh, K.C., and C.H. Liu, Evolution of atmospheric spectrum by processes of wave-wave interaction, *Radio Sci.*, **20**, 1279-1294, 1985.

Yih, C.S., Stability of two-dimensional parallel flows for three-dimensional disturbances, *Q. Appl. Math.*, **12**, 434-435, 1955.